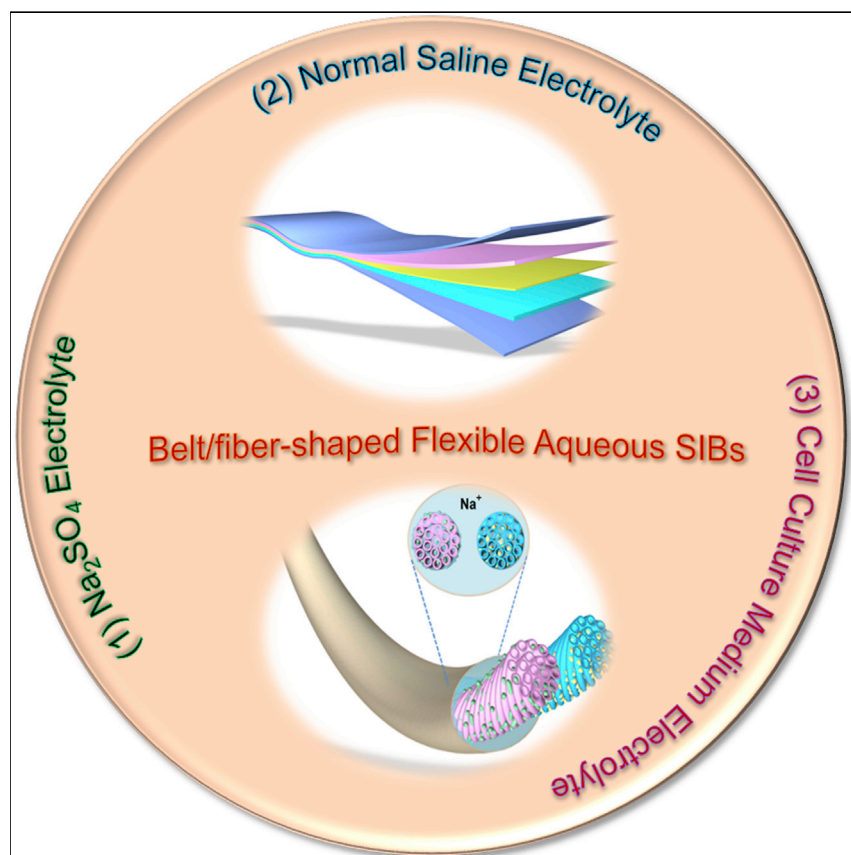


Article

Multi-functional Flexible Aqueous Sodium-Ion Batteries with High Safety



Flexible aqueous sodium-ion batteries (SIBs), using Na_2SO_4 , normal saline, or cell-culture medium as the electrolyte, are introduced as energy storage devices with potential application in wearable and implantable electric devices and biological and medical fields.

Zhaowei Guo, Yang Zhao, Yuxue Ding, ..., Yongyao Xia, Huisheng Peng, Yonggang Wang

penghs@fudan.edu.cn (H.P.)
ygwang@fudan.edu.cn (Y.W.)

HIGHLIGHTS

Flexible aqueous belt- and fiber-shaped SIBs with high safety are fabricated

Normal saline and cell-culture medium are used directly as electrolytes for SIBs

Fiber-shaped SIBs exhibit an electrochemical deoxygenation function



Guo et al., Chem 3, 348–362
August 10, 2017 © 2017 Elsevier Inc.
<http://dx.doi.org/10.1016/j.chempr.2017.05.004>

Article

Multi-functional Flexible Aqueous Sodium-Ion Batteries with High Safety

Zhaowei Guo,^{1,3} Yang Zhao,^{2,3} Yuxue Ding,² Xiaoli Dong,¹ Long Chen,¹ Jingyu Cao,² Changchun Wang,² Yongyao Xia,¹ Huisheng Peng,^{2,*} and Yonggang Wang^{1,4,*}

SUMMARY

Flexible energy storage devices are attracting extensive attention, but most of the reported flexible batteries and supercapacitors use either strong acid or base or toxic flammable organic solutions as electrolytes, which pose potential safety issues when worn by humans or implanted into the body. Here, we present a highly safe family of flexible sodium-ion batteries (SIBs) based on a $\text{Na}_{0.44}\text{MnO}_2$ cathode, a nano-sized $\text{NaTi}_2(\text{PO}_4)_3$ @C anode, and various aqueous electrolytes containing Na^+ . The resulting belt- and fiber-shaped aqueous SIBs exhibit high volumetric energy and power density, high flexibility, and long life and thus can be safely applied in wearable electronic devices. When normal saline or cell-culture medium is used as the electrolyte, these SIBs can still work well, indicating potential application in implantable electronic devices. The fiber-shaped electrodes in Na^+ -containing aqueous electrolytes exhibit an electrochemical deoxygenation function, which could be applied in biological and medical fields.

INTRODUCTION

Nowadays, the demand for flexible, wearable, and even implantable electrical devices, such as intelligent bracelets, wearable sensors, implantable clinical devices, and electric pills,^{1–4} has led to an upsurge in the development of corresponding energy storage systems for power supply.^{5–8} To meet this target, energy storage systems must satisfy several requirements; they must be non-toxic, flexible, and light weight and have high mechanical strength and good biocompatibility. However, the traditional rechargeable batteries and supercapacitors currently available^{9,10} cannot satisfy the requirement for flexible electrical devices because of their stiff current collector and rigid assembly. Tremendous efforts have been made to develop adequate flexible systems.^{5–8,11} As a result, various belt- and fiber-shaped flexible Li-ion batteries (LIBs),^{12–20} Li-S batteries,^{21–23} Li-O₂ batteries^{24,25} and supercapacitors^{26–32} have been developed recently. Unfortunately, the electrolytes used in these flexible batteries or supercapacitors are mainly based on strong acid or base or toxic and flammable organic solutions,^{12–18,21–30} which pose a huge potential safety hazard when carried around or worn by humans, let alone implanted into human bodies. Repeated bending of these flexible power sources is likely to lead to leakage of electrolyte.

In recent years, sodium-ion batteries (SIBs) have been attracting extensive attention as a promising alternative to LIBs because they benefit from abundant natural reserves and the low cost of sodium.^{33,34} Given their similar mechanism of operation (i.e., Na^+ or Li^+ intercalation or de-intercalation), the fabrication technologies for conventional LIBs, such as a stiff current collector, rigid assembly, and organic

The Bigger Picture

The development of wearable and implantable electrical devices has been in great demand recently. However, most existing energy storage systems are based on strong corrosive or toxic electrolytes, posing a huge safety hazard as a result of solution leakage. Here, we have developed a family of safe and flexible belt- and fiber-shaped aqueous sodium-ion batteries (SIBs) by using various Na^+ -containing aqueous electrolytes, including Na_2SO_4 solution, normal saline, and cell-culture medium. The resulting SIBs exhibit high flexibility and excellent electrochemical performance and can be safely applied in wearable electronics. Flexible SIBs with normal saline or cell-culture medium as the electrolyte showed excellent performance, indicating potential application in implantable electronic devices. In addition, the fiber-shaped electrode in normal saline or cell-culture medium electrolyte can consume O_2 and change the pH, implying promising application in biological and medical investigations.

electrolyte, can be used directly for the development of ordinary SIBs. Although some efforts have been made to develop flexible electrodes for SIBs,^{35–40} the corresponding flexible devices are still rarely reported. The most reported SIBs are still based on toxic and flammable organic electrolytes. Theoretically, SIBs based on Na⁺-containing aqueous electrolytes (i.e., aqueous SIBs) are suitable for powering wearable devices and implantable clinical devices, e.g., a pressure monitor, ion concentration meter, and electric pill, as a result of the inherent biocompatibility and safety of Na⁺-containing aqueous solutions. It is also expected that an aqueous SIB can be built with cell-culture medium (which principally contains Na⁺ and water), which potentially opens a new door for the development of implantable devices for biological and/or medical investigations. Unfortunately, flexible aqueous SIBs are not yet available, although some conventional aqueous SIBs for grid-scale energy storage have been reported.^{41,42}

Here, we have developed a family of flexible belt- and fiber-shaped aqueous SIBs by using electrodes based on Na_{0.44}MnO₂ (NMO) and nano-sized carbon-coated NaTi₂(PO₄)₃ (NTPO@C) as the cathode and anode, respectively, in various Na⁺-containing aqueous electrolytes. The belt-shaped aqueous SIB was fabricated with a lamination structure containing NMO, NTPO@C electrodes, and an electrolyte-drenched separator through a vacuum sealing process. The fiber-shaped aqueous SIB employed aligned carbon nanotube (CNT)/NMO and CNT/NTPO@C hybrid fibers as electrodes, in which the active materials (NMO or NTPO@C) were closely incorporated within the aligned CNT fibers by a wet twist process. Both the belt- and fiber-shaped NMO/NTPO@C aqueous SIBs using Na₂SO₄ electrolyte delivered high volumetric energy and power density, high flexibility, excellent rate performance, and good cycling stability. Furthermore, these flexible SIBs could still work well when normal saline or cell-culture medium (Dulbecco's modified Eagle's medium [DMEM]) was used directly as their electrolyte. Finally, the deoxygenation behavior arising from the side reaction of O₂ electrochemical reduction was also investigated in detail.

RESULTS

Preparation and Characterization of Electrode Materials

The electrode materials of NMO and nano-sized NTPO@C were prepared by a conventional solid-state method and a sol-gel method, respectively (see [Experimental Procedures](#)). X-ray diffraction (XRD) patterns and scanning electron microscopy (SEM) images of the as-prepared electrode materials are shown in [Figures S1](#) and [S2](#). The carbon content (~11 wt %) of NTPO@C was confirmed by thermogravimetry (TG) analysis ([Figure S3](#)). The carbon layer was about 2 nm thick according to the transmission electron microscopy (TEM) image ([Figure S4](#)). Before fabrication of the full cell, the electrochemical profiles of the NMO film electrode and the NTPO@C film electrode in aqueous electrolyte (1 M Na₂SO₄) were investigated, respectively, by cyclic voltammetry (CV) and galvanostatic charge-discharge measurements with a typical three-electrode system (a Ag/AgCl electrode [$E = 0.1971$ V versus SHE] was used as the reference electrode, and an activated carbon film electrode served as the counter electrode). As shown in [Figure S5A](#), it can be detected from the CV curves that the NMO electrode exhibited three pairs of redox peaks at +0.17/+0.07 V, +0.37/+0.28 V, and +0.58/+0.51 V (versus Ag/AgCl), corresponding to Na⁺ de-intercalation on positive sweep and Na⁺ intercalation on negative sweep.⁴³ The reversible Na⁺ intercalation and de-intercalation of NTPO@C occurred at -0.86 and -0.7 V (versus Ag/AgCl) ([Figure S5B](#)). According to galvanostatic charge-discharge measurements tested at a current density of

¹Department of Chemistry and Shanghai Key Laboratory of Molecular Catalysis and Innovative Materials, Institute of New Energy, iChEM (Collaborative Innovation Center of Chemistry for Energy Materials), Fudan University, Shanghai 200433, China

²State Key Laboratory of Molecular Engineering of Polymers, Department of Macromolecular Science and Laboratory of Advanced Materials, Fudan University, Shanghai 200438, China

³These authors contributed equally

⁴Lead Contact

*Correspondence: penghs@fudan.edu.cn (H.P.), ygwang@fudan.edu.cn (Y.W.)

<http://dx.doi.org/10.1016/j.chempr.2017.05.004>

0.2 A g⁻¹ (Figures S6A and S6B), the NMO and NTPO@C electrodes displayed a specific capacity of 45 mAh g⁻¹ in the potential window of 0–0.7 V (versus Ag/AgCl) and a specific capacity of 80 mAh g⁻¹ in the potential window of 0 to –0.9 V (versus Ag/AgCl), respectively. The capacity retention of both electrodes over 200 cycles was 90% (NMO) and 85% (NTPO@C), respectively (Figures S6C and S6D).

Fabrication and Electrochemical Profile of Belt-Shaped Aqueous SIBs

After the three-electrode investigations, we used the NMO- and NTPO@C-based electrodes as cathode and anode, respectively, to fabricate a belt-shaped flexible full cell with an aqueous electrolyte of 1 M Na₂SO₄. We used the fabrication technology for flexible aqueous LIBs, which we recently reported,²⁰ to build the aqueous SIBs. The flexible cathode or anode was prepared directly with a mixture of NMO (or NTPO@C) as active materials, acetylene black (AB) as the conductive agent, and polytetrafluoroethylene (PTFE) as the binder into a film, which was then pressed on a flexible and lightweight stainless steel mesh to form a flexible electrode (Figures S7 and S8). A microporous polyacrylonitrile (PAN) nonwoven separator wetted by electrolyte (1 M Na₂SO₄) was used to separate the as-prepared NMO cathode and NTPO@C anode to form a flexible SIB through a sealing process (Figure 1A). As shown in Figure 1B, the belt-shaped SIB exhibited high mechanical strength and integrity after undergoing repeated bending. The full cell could be cycled between 0 and 1.6 V with three voltage plateaus at ~1.3, 1.1, and 0.9 V. The full cell delivered a specific capacity of 43 mAh g⁻¹ at a current density of 0.1 A g⁻¹ (Figures 1C and 1D); the current density and capacity were all calculated on the basis of the mass of the cathode material (i.e., NMO). Even at a much higher current density of 5 A g⁻¹, the capacity could still be kept at about 27 mAh g⁻¹ (equivalent to 63% of the former), indicating an excellent rate capability (Figures 1C and 1D). The cycle profile of the full cell tested at a current density of 0.2 A g⁻¹ is given in Figure 1E. It can be seen that the initial specific capacity of the full cell was about 42 mAh g⁻¹, which gradually decreased to 26 mAh g⁻¹ after 1,000 cycles as the coulombic efficiency approached 100%, exhibiting a capacity retention of 60%. The mass energy and power density of the aqueous SIB were calculated on the basis of the corresponding charge-discharge data and the total mass of the electrode materials (NMO + NTPO@C), which is given as a Ragone plot profile (Figure S9A). As shown in Figure S9A, the cell delivered a maximum mass energy density of 30 Wh kg⁻¹ and a maximum mass power density of 4,678 W kg⁻¹. The mass energy and power density of the flexible aqueous SIB were also calculated on the basis of the total mass of the device (including active materials, current collectors, electrolyte, and packaging), which was about 10% of the value calculated on the basis of the active materials (Figure S9B). When converted into areal energy and power density, the data were 0.47 mWh cm⁻² and 74.5 mW cm⁻², respectively (Figure S9C). It is well known that volumetric energy and power densities are very important for wearable power sources. As a result, we further converted the achieved areal energy and power densities into volumetric energy and power densities by considering the 0.2 mm thickness of the packaged flexible and belt-shaped SIB (Figure S10). As shown in Figure 1F, the maximum volumetric energy density and power density reached 23.8 mWh cm⁻³ and 3.8 W cm⁻³, respectively, which are much higher than most reported flexible and wearable LIBs or supercapacitors (see Table S1 for detailed information). The detailed calculations for the volumetric energy and power density are given in the [Supplemental Information](#).

We investigated the retention capacity of the flexible belt-shaped aqueous SIB under bending and mechanical fatigue states by bending it 100 times at different

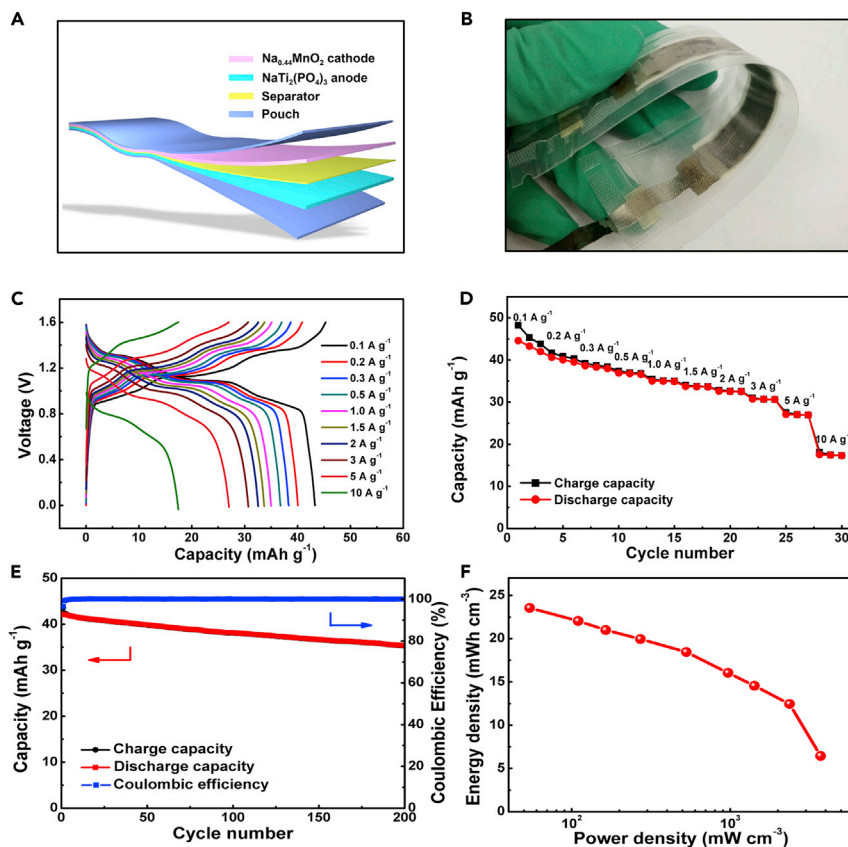


Figure 1. Fabrication and Electrochemical Profile of the Flexible Belt-Shaped $\text{Na}_{0.44}\text{MnO}_2//\text{NaTi}_2(\text{PO}_4)_3@\text{C}$ Battery Using 1 M Na_2SO_4 as Electrolyte

(A) Schematic illustration of the structure of the battery.
 (B) Photo profile of an as-prepared belt-shaped aqueous SIB.
 (C and D) Galvanostatic charge-discharge curves (C) and capacity stability at different current densities (D) of the belt-shaped aqueous SIB.
 (E) Cycling performance of the belt-shaped aqueous SIB tested at a current density of 0.2 A g^{-1} .
 (F) Ragone plot (volumetric energy density versus power density) of the belt-shaped aqueous SIB.

angles and to form a circle. Figures 2A–2F show the galvanostatic charge-discharge curves for the flexible belt-shaped SIB under different bending conditions, including before bending (flat) and bending 100 times each to 45° , 90° , 135° , 180° , and a circle. The belt-shaped SIBs were remained bent during the test procedure. Almost no decay in capacity or increase in polarization was detected under different bending conditions. The corresponding cycling stability results are presented in Figure 2G. It can be seen that the belt-shaped SIB lost receivable capacity with each repeated bending angle. The loss of capacity can be attributed to the fact that repeated bending destroyed the tight contact of the anode, separator, and cathode step by step, which thus increased the impedance of the battery. As a demonstration of an application, two such belt-shaped SIBs were connected in series to power a red-light-emitting diode (Figure S11).

Preparation and Electrochemical Performance of Fiber-Shaped Aqueous SIBs

In addition to two-dimensional (2D) flexible power sources, one-dimensional (1D) flexible power sources based on fiber-shaped electrodes, such as fiber-shaped LIBs^{13,14} and supercapacitors,^{26–29,44} have been attracting extensive attention

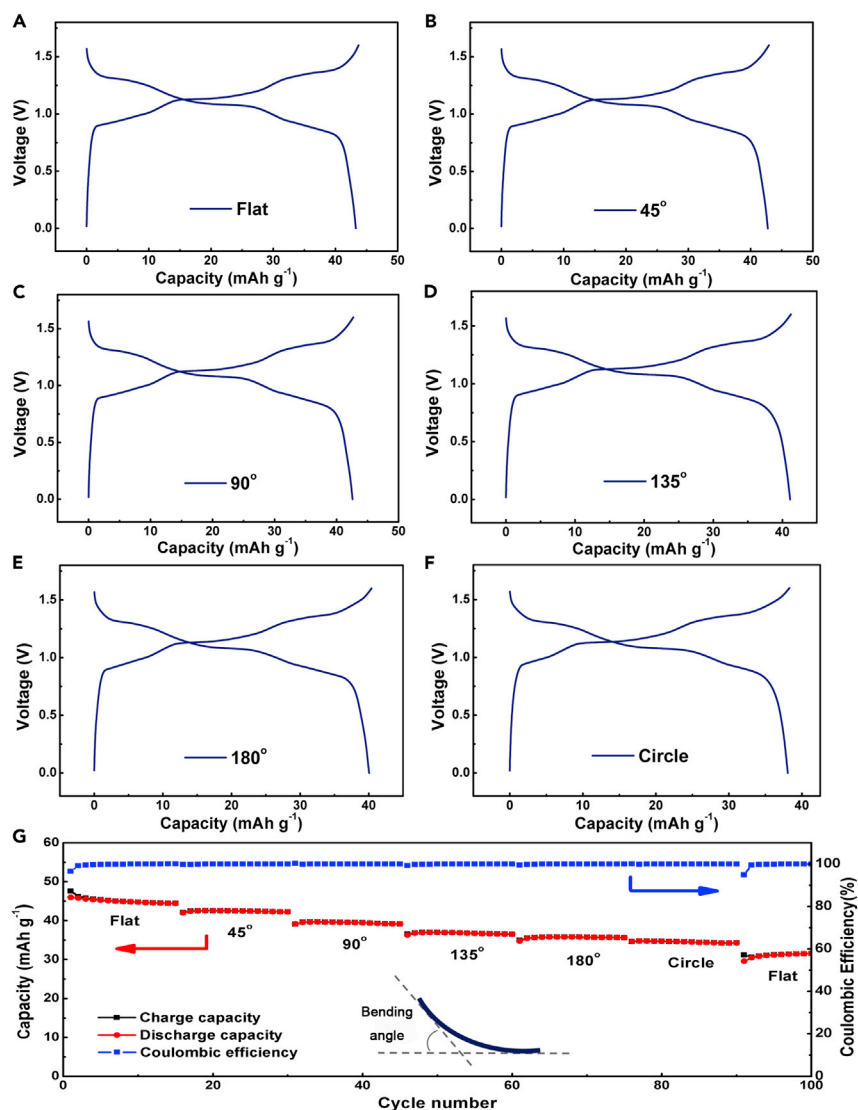


Figure 2. Electrochemical Performance of the Belt-Shaped Aqueous SIB at Different Bending States

(A–F) Before bending (A), bent at of 45° (B), 90° (C), 135° (D), and 180° (E), and bent to a circle (F). (G) Cycling profile under different bending conditions tested at a current density of 0.2 A g⁻¹.

recently because 1D electrodes can be directly integrated into daily necessities, such as in clothes, caps, and gloves. Furthermore, the micro-sized 1D electrode potentially facilitates implantable applications, especially in the human body. Aligned carbon nanotube (CNT) fibers are a good candidate for flexible batteries because of the high flexibility, tensile strength (at the level of 10²–10³ MPa),⁴⁵ and high electrical conductivity (in the order of 10²–10³ S/cm).⁴⁶ Therefore, the NMO and NTPO@C were combined with the aligned CNT fibers to form the fiber-shaped electrodes. In this approach, the spinnable CNT arrays (Figure S12) were first synthesized by the chemical vapor deposition method (see detailed preparation process in the Experimental Procedures), and the aligned CNT sheets (Figure S13) were continuously pulled out of the CNT array with a knife touching the top edge. The detailed preparation process for aligned CNT sheets is shown in Figure S14.⁴⁷ NMO and

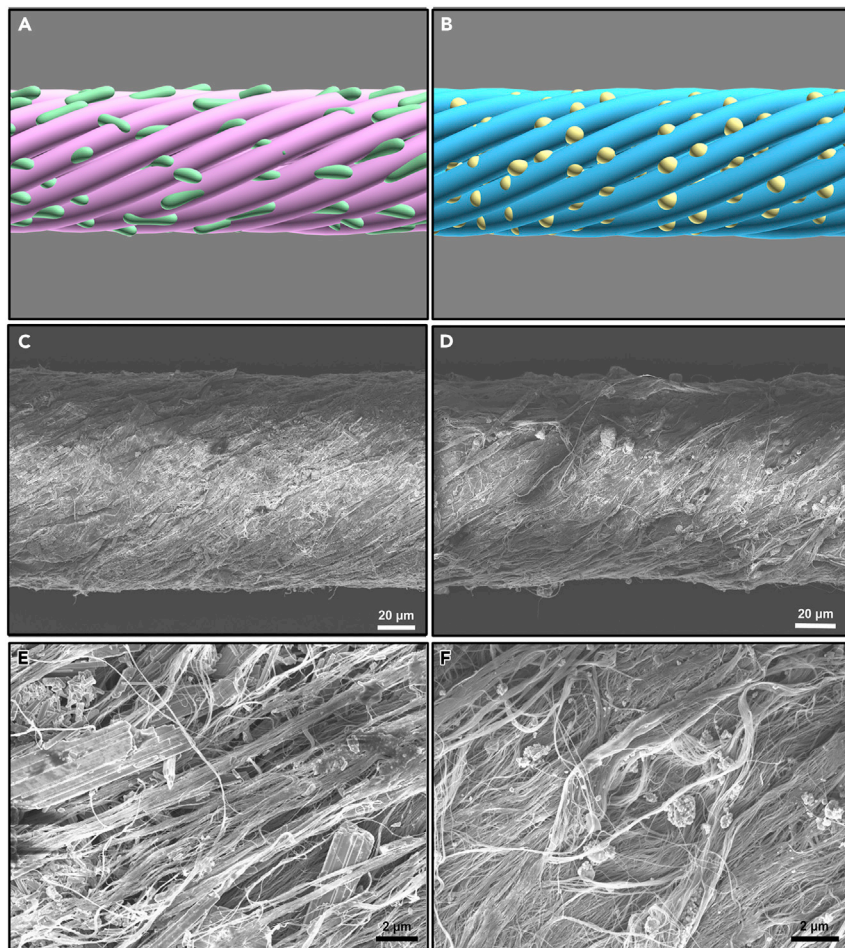


Figure 3. Characterization of CNT/Na_{0.44}MnO₂ and CNT/NaTi₂(PO₄)₃@C Fiber-Shaped Electrodes

(A and B) Schematic illustration of hybrid electrodes CNT/Na_{0.44}MnO₂ (A) and CNT/NaTi₂(PO₄)₃@C (B). (C–F) SEM images at different magnifications of hybrid electrodes CNT/Na_{0.44}MnO₂ (C and E) and CNT/NaTi₂(PO₄)₃@C (D and F).

NTPO@C nanoparticles were dispersed and attached to the CNT sheets and then twisted into fiber-shaped electrodes (Figures 3A and 3B; see detailed preparation process in the [Experimental Procedures](#)). The SEM images of the aligned CNT/NMO (92.5 wt % for NMO) and aligned CNT/NTPO@C (83.1 wt % for NTPO@C) composite electrodes are shown in Figures 3C and 3D, respectively; they demonstrate uniform diameters of approximately 110 and 100 μm, respectively. The NMO and NTPO@C particles were well wrapped within the aligned CNT bundles (Figures 3E and 3F). There were no extra conductive agents or metal current collectors in the fiber-shaped electrodes. The highly flexible and bendable characteristics of the free-standing CNT-based hybrid electrodes are demonstrated in [Figure S15](#).

The electrochemical profiles of the fiber-shaped CNT/NMO and CNT/NTPO@C electrodes were investigated with three-electrode systems in 1 M Na₂SO₄ solution (Figures S16 and S17) before the fabrication of the full cell. We then prepared the 1D flexible aqueous SIBs by putting the fiber-shaped electrodes directly in a tube containing aqueous electrolyte (Figure 4A). The aqueous electrolyte (1 M Na₂SO₄)

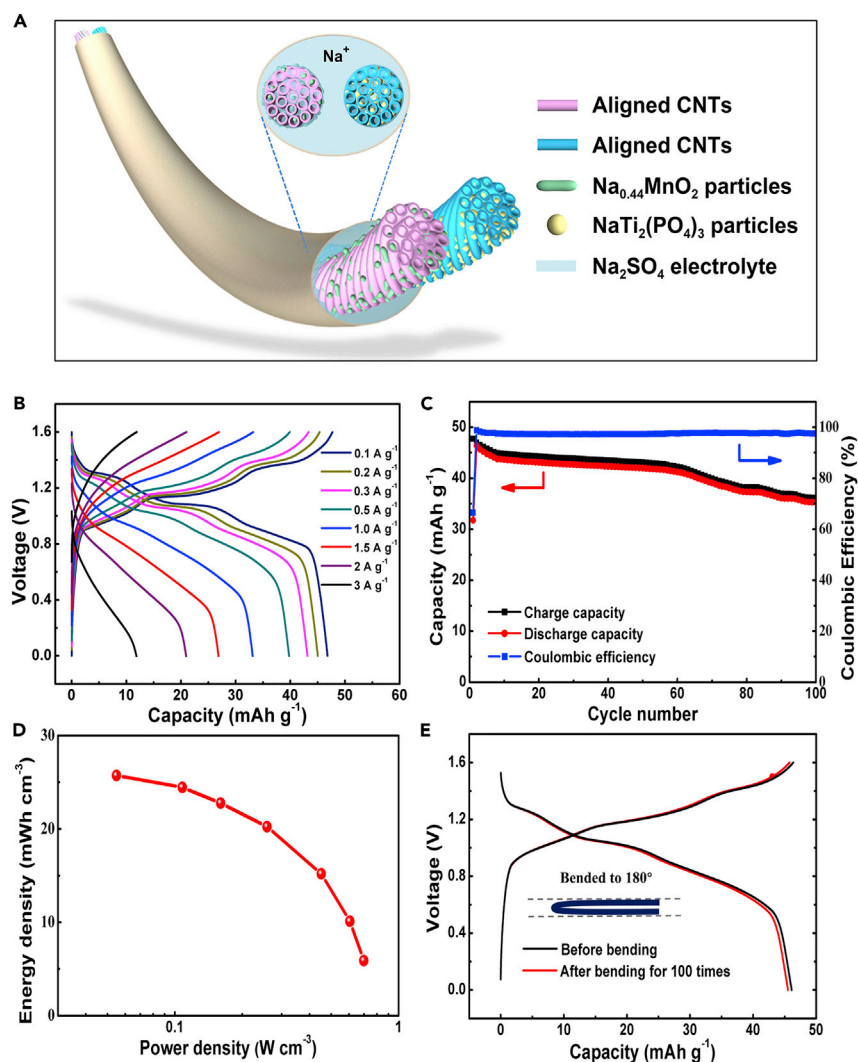


Figure 4. Schematic Image and Electrochemical Profile of the Flexible Fiber-Shaped $\text{Na}_{0.44}\text{MnO}_2/\text{NaTi}_2(\text{PO}_4)_3@\text{C}$ Battery Using 1 M Na_2SO_4 as Electrolyte

(A) Schematic illustration of the structure of the battery.
 (B and C) Galvanostatic charge-discharge curves (B) and capacity stability (C) at different current densities of the fiber-shaped aqueous SIB.
 (D) Ragone plot (volumetric energy density versus power density) of the fiber-shaped aqueous SIB.
 (E) Galvanostatic charge-discharge curves before and after bending of the flexible fiber-shaped aqueous SIB at a current density of 0.2 A g^{-1} . The aqueous electrolyte (1 M Na_2SO_4) used for the fiber-shaped SIB was pre-treated with a flow of N_2 for the removal of dissolved O_2 , as explained in Figure 6.

used for the fiber-shaped SIB was pre-treated with a flow of N_2 for the removal of the dissolved O_2 , which is explained in the last section. The galvanostatic charge-discharge curves of the SIB tested in 1 M Na_2SO_4 electrolyte in the potential window of 0–1.6 V are shown in Figure 4B. The full cell delivered a discharge specific capacity of 46 mAh g^{-1} (on the basis of the mass of the cathode material, i.e., NMO) at a current density of 0.1 A g^{-1} , which is in accordance with that of the belt-shaped SIB. At the high applied current density of 3 A g^{-1} , the fiber-shaped SIB still delivered a capacity of 12 mAh g^{-1} (Figure 4B), indicating a good rate capability. The cycle profile of the aqueous SIB tested at a current density of 0.2 A g^{-1} is shown in Figure 4C,

which demonstrates that the capacity of the full cell was still maintained at 76% of that in the initial cycle even after 100 cycles. The Ragone plot shown in Figure 4D was derived from galvanostatic charge-discharge capacity data. The fiber-shaped aqueous SIB delivered an energy density of 25.7 mWh cm^{-3} at a specific power density of 0.054 W cm^{-3} . A respectable energy density of 5.9 mWh cm^{-3} was reached at a high power density of 0.7 W cm^{-3} . The flexibility of the fiber-shaped aqueous SIB was also investigated. The galvanostatic charge-discharge curves of the fiber-shaped aqueous SIB before and after bending are shown in Figure 4E. Even after bending at 180° for 100 times, the galvanostatic charge-discharge curves of the battery remained almost unchanged, also indicating a high flexibility of the fiber-shaped aqueous SIB.

Belt- and Fiber-Shaped Aqueous SIBs Using Normal Saline or DMEM as Electrolyte

In the above sections, the electrochemical performance and flexible characteristics of belt- and fiber-shaped SIBs using $1 \text{ M Na}_2\text{SO}_4$ were investigated in detail. Because of the inherent safe and environment friendly nature of Na_2SO_4 solution, these flexible aqueous SIBs can be used as the power source for wearable electronic devices without concern for electrolyte leakage under repeated bending conditions. However, it is still highly desirable to use biocompatible electrolytes for these aqueous SIBs to satisfy the requirement of implantable electronic devices for humans. Accordingly, we used normal saline (0.9 wt % NaCl) and cell-culture medium (DMEM) (see Table S2 for ingredients) as electrolytes to fabricate the belt- and fiber-shaped SIBs. We also note that we pre-treated the normal saline or DMEM used for the fiber-shaped SIB with a flow of N_2 to eliminate the dissolved O_2 , as explained in the last section. As shown in Figures 5A and 5B, the belt- and fiber-shaped SIBs using normal saline electrolytes exhibited galvanostatic charge-discharge curves with three voltage plateaus, similarly to those tested in $1 \text{ M Na}_2\text{SO}_4$ electrolyte. The specific capacities for belt- and fiber-shaped SIBs using normal saline electrolyte were 41 and 37 mAh g^{-1} , respectively, at a current density of 0.2 A g^{-1} (both specific capacity and current density were calculated on the basis of the mass of the cathode material, i.e., NMO), which are slightly smaller than those tested in $1 \text{ M Na}_2\text{SO}_4$ electrolyte. The reduction of capacity is attributable to the lower Na^+ concentration (0.9 wt. %) in normal saline electrolyte than in $1 \text{ M Na}_2\text{SO}_4$. When DMEM was used as the electrolyte, belt-shaped SIB maintained their charge-discharge profile with three voltage plateaus and a specific discharge capacity of 40 mAh g^{-1} (Figure 5C), which is almost the same as that achieved in normal saline electrolyte. However, with the DMEM electrolyte, fiber-shaped SIBs exhibited a much lower capacity of 32 mA g^{-1} (Figure 5D). Furthermore, the voltage gap between charge and discharge was also larger than that in normal saline electrolyte. In addition, the fiber-shaped SIBs using normal saline or DMEM as electrolyte exhibited lower coulombic efficiency than those using $1 \text{ M Na}_2\text{SO}_4$ electrolyte (see Figures 4B, 5B, and 5D). This can be attributed to the fact that the Na-storage (i.e., Na-intercalation) potential of the $\text{NaTi}_2(\text{PO}_4)_3$ anode in $1 \text{ M Na}_2\text{SO}_4$ is just a little above the hydrogen evolution potential, and the lower Na^+ concentration in normal saline or DMEM (about 0.15 or 0.11 M Na^+ , respectively) results in the negative shift of the Na^+ -intercalation potential according to the Nernst equation, which is thus closer to the hydrogen evolution potential. In other words, when normal saline or DMEM is used as the electrolyte, the undesired hydrogen evolution reaction is more serious than that in $1 \text{ M Na}_2\text{SO}_4$ electrolyte. On the other hand, CNT-based fiber-shaped electrodes are more sensitive to the composition of the electrolyte than film electrodes because of the inherent catalytic activity of CNTs, which is further clarified in the next section. In brief, the flexible SIBs using normal saline or DMEM as

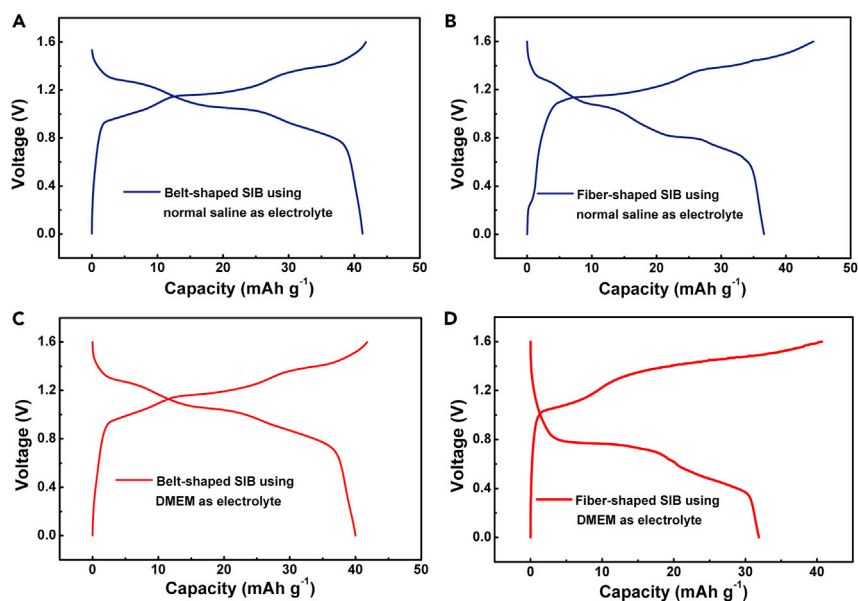


Figure 5. Electrochemical Profile of the Belt- and Fiber-Shaped $\text{Na}_{0.44}\text{MnO}_2//\text{NaTi}_2(\text{PO}_4)_3@C$ Batteries Using Normal Saline or Cell Culture Medium as the Electrolyte

(A and B) Galvanostatic charge-discharge curves of the belt-shaped (A) and fiber-shaped (B) aqueous SIBs using normal saline as the electrolyte tested at a current density of 0.2 A g^{-1} . (C and D) Galvanostatic charge-discharge curves of the belt-shaped (C) and the fiber-shaped (D) aqueous SIBs using DMEM as the electrolyte tested at a current density of 0.2 A g^{-1} . The aqueous electrolytes (normal saline and DMEM) used for the fiber-shaped SIBs were pre-treated with a flow of N_2 for the removal of dissolved O_2 , as explained in Figure 6.

electrolyte should be quite safe when applied to implantable electronic devices, circumventing the most important safety hazard as a consequence of electrolyte leakage during bending conditions.

Deoxygenation Function of Fiber-Shaped Aqueous SIBs

As mentioned above, the aqueous electrolyte for fiber-shaped SIBs must be pre-treated with a flow of N_2 for the removal of the dissolved O_2 . However, for belt-shaped SIBs, it is not necessary to eliminate the dissolved O_2 . The key reason for this difference is attributed to the fact that the CNT fibers have catalytic activity for O_2 electrochemical reduction, as demonstrated in our previous report.⁴⁸ In order to clarify this point, we investigated fiber-shaped SIBs using pristine normal saline or DMEM as electrolyte (without pre-treatment of N_2) with galvanostatic charge-discharge tests at a current density of 0.2 A g^{-1} (Figures 6A and 6B). As shown in Figures 6A and 6B, the charge voltages of both fiber-shaped SIBs were lower than 1.0 V, whereas the charge voltages of the fiber-shaped SIBs using the electrolyte without O_2 reached 1.6 V (Figures 4B and 5). The corresponding discharge capacities of both SIBs were almost zero (Figures 6A and 6B), indicating a huge irreversibility.

Theoretically, the charge process of the fiber-shaped SIB depends on Na^+ de-intercalation in the cathode ($\text{Na}_{0.44}\text{MnO}_2 \rightarrow \text{Na}_{0.44-x}\text{MnO}_2 + x\text{Na}^+ + xe^-$) and Na^+ intercalation in the anode ($\text{NaTi}_2(\text{PO}_4)_3 + x\text{Na}^+ + xe^- \rightarrow \text{Na}_{1+x}\text{Ti}_2(\text{PO}_4)_3$). Its discharge reverses the charge process. However, if O_2 is present in the electrolyte, the Na^+ -intercalation reaction in the anode can be replaced by O_2 electrochemical catalytic reduction ($0.5\text{O}_2 + \text{H}_2\text{O} + 2e^- \rightarrow 2\text{OH}^-$). To demonstrate this assumption, we

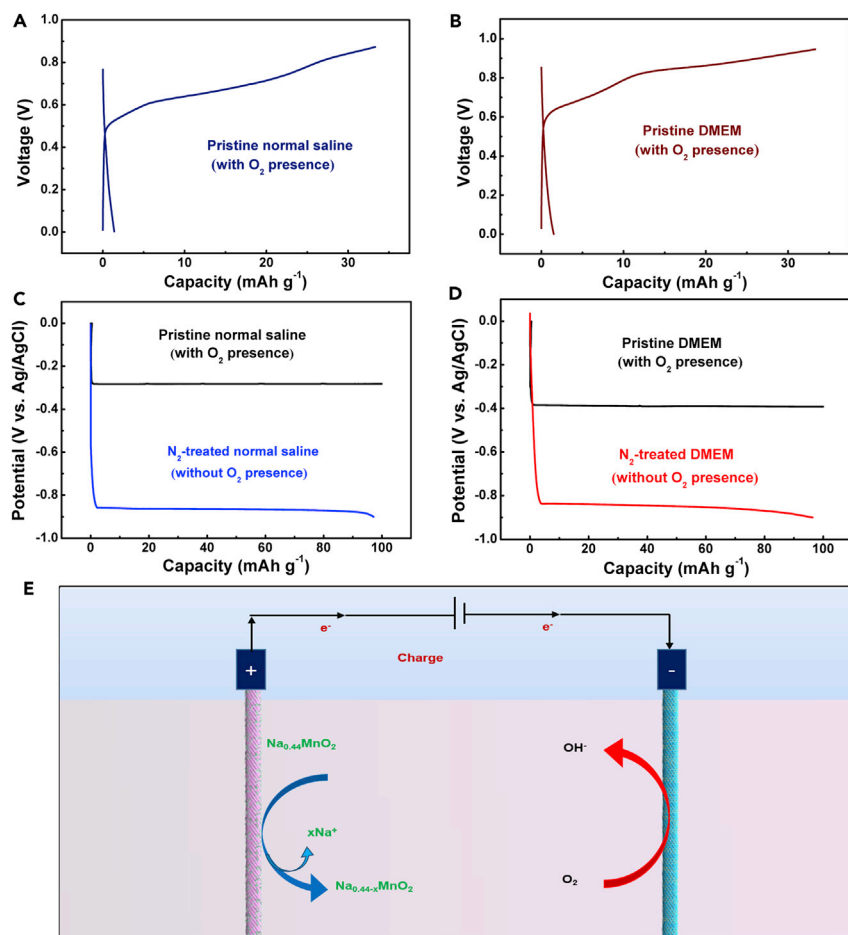


Figure 6. Electrochemical Deoxygenation Function of Fiber-Shaped Aqueous SIBs

(A and B) Galvanostatic charge-discharge curves at a current density of $0.2\ A\ g^{-1}$ of the fiber-shaped SIBs using pristine normal saline (with O_2) (A) and pristine DMEM (with O_2) (B) as electrolyte. The charge time was controlled at 10 min for preventing the oxygen evolution reaction.

(C) Discharge curves (tested at a current density of $0.2\ A\ g^{-1}$) of the fiber-shaped CNT/ $NaTi_2(PO_4)_3@C$ hybrid electrodes in pristine normal saline solution with O_2 (black line) and in N_2 -treated normal saline solution without O_2 (blue line).

(D) Discharge curves (tested at a current density of $0.2\ A\ g^{-1}$) of the fiber-shaped CNT/ $NaTi_2(PO_4)_3@C$ hybrid electrodes in pristine DMEM solution with O_2 (black line) and in N_2 -treated DMEM solution without O_2 (red line).

(E) Schematic showing the operation mechanism of the deoxygenation function of the fiber-shaped aqueous SIB. The CNTs have catalytic activity for O_2 electrochemical reduction, which was demonstrated in our previous report.⁴⁸

investigated Na^+ intercalation behavior (i.e., discharge) of NTPO@C-based fiber-shaped electrodes in pristine normal saline and DMEM (with dissolved O_2) and normal saline and DMEM treated with a flow of N_2 (without dissolved O_2) by using a three-electrode system (a Ag/AgCl electrode [$E = 0.1971\ V$ versus SHE] as the reference electrode and an activated carbon electrode as the counter electrode). As shown in Figures 6C and 6D, the NTPO@C-based fiber-shaped electrodes exhibited infinite discharge plateaus at around -0.3 and $-0.4\ V$ (versus Ag/AgCl) in pristine normal saline and pristine DMEM electrolyte, respectively, as a result of the electrochemical reduction of dissolved O_2 . However, when tested in normal saline and DMEM electrolyte pre-treated with a flow of N_2 , the NTPO@C-based

fiber-shaped electrodes displayed finite discharge plateaus (about 100 mAh g⁻¹ calculated on the basis of the mass of NTPO@C) at around -0.9 V (versus Ag/AgCl) according to the typical Na⁺ intercalation in the NTPO@C electrode. The comparison in Figures 6C and 6D confirms the side reaction of an O₂ reaction on the NTPO@C-based fiber-shaped electrode when there is dissolved O₂ in the electrolyte. However, the electrochemical behavior of NMO is not affected by the presence of O₂ (Figure S18).

According to the above results (Figures 6C, 6D, and S18), the charge process of fiber-shaped SIBs (Figures 6A and 6B) involves Na⁺ de-intercalation [Na_{0.44}MnO₂ → Na_{0.44-x}MnO₂ + xNa⁺ + xe⁻] in the cathode and an O₂ reduction reaction [0.5O₂ + H₂O + 2e⁻ → 2OH⁻] in the anode, which is illustrated in Figure 6E. The consumption of oxygen and change in the pH of the electrolyte during the discharge process (i.e., O₂ electrochemical reduction) on the NTPO@C anode, corresponding to the charge process of the fiber-shaped SIB, can be considered an electrochemical deoxygenation process for the electrolyte. Undoubtedly, the side reaction of O₂ reduction is a disadvantage for an aqueous battery, resulting in huge irreversibility of the charge-discharge cycle. However, when implanted in the human body, such an electrochemical deoxygenation process (O₂ consumption and pH adjustment shown in Figure 6E) of fiber-shaped electrodes could be applied to biological investigations and medical therapy. For example, very recently, Zhang et al.⁴⁹ successfully used the chemical deoxygenation reaction of polymer-modified magnesium silicide (Mg₂Si) nanoparticles (Mg₂Si + 4H⁺ + 2O₂ → 2Mg²⁺ + 2H₂O + SiO₂) to realize cancer starvation therapy. Thus, it can be expected that the electrochemical deoxygenation function of fiber-shaped electrodes in normal saline, cell-culture medium, and body fluid containing Na⁺ could be used for the same task.

DISCUSSION

As mentioned in the Introduction, the demand for flexible, wearable, and even implantable electrical devices requires flexible power sources with high safety. As a result, flexible batteries and supercapacitors are attracting extensive attention. However, most of the reported flexible batteries and supercapacitors use either strong acid or base or toxic flammable organic solutions as electrolytes, which pose potential safety issues when worn by humans or implanted into the body. In this work, aqueous SIBs based on aqueous electrolyte solutions containing Na⁺ were introduced to flexible energy storage devices. It has been demonstrated that belt- and fiber-shaped aqueous SIBs using 1 M Na₂SO₄ display promising electrochemical performance, including high volumetric energy and power density, high flexibility, excellent rate ability, and a long cycle life, and thus can be considered safe power sources for wearable electrical devices. Furthermore, biocompatible normal saline and cell-culture medium (DMEM) can also be used as electrolytes for these flexible SIBs, which provides an opportunity for their use in implantable electronic devices.

On the other hand, it was demonstrated that the side reaction of O₂ electrochemical reduction on the fiber-shaped electrode could consume O₂ in normal saline or DMEM solution, which could be considered as a typical deoxygenation process. For instance, very recently, Zhang et al.⁴⁹ successfully used the chemical deoxygenation reaction of polymer-modified magnesium silicide (Mg₂Si) nanoparticles for cancer starvation therapy. Accordingly, it can be expected that the deoxygenation of fiber-shaped electrodes in biocompatible solutions (such as normal saline, DMEM solution, or even body fluid) could be applied in biological and medical

investigations, which potentially highlights a new field of application for flexible aqueous SIBs, as well as power sources.

EXPERIMENTAL PROCEDURES

Materials

$\text{Na}_{0.44}\text{MnO}_2$ was prepared by the solid-state method according to previous reports.^{43,50,51} In a typical synthesis, Mn_3O_4 and Na_2CO_3 were mixed by ball-milling treatment at 300 rpm for 10 hr in a molar ratio of 1:0.726. The mixture was reacted at 500°C in air for 5 hr. The precursor was then ball milled for another 10 hr and then heated at 900°C in air for another 12 hr. Nano-sized carbon-coated $\text{NaTi}_2(\text{PO}_4)_3$ was synthesized by a sol-gel method.^{52,53} 2 g PVA (polyvinyl ethanol) was dissolved in 100 mL of H_2O under heating, and then 0.0051 mol Na_2CO_3 (2% excess; the extra amount of Na was added to compensate for the loss of Na, i.e., volatilization of Na salt, during the high-temperature synthesis process), 0.02 mol TiO_2 , and 0.03 mol $\text{NH}_4\text{H}_2\text{PO}_4$ were added to the PVA aqueous solution to form a homogeneous and transparent solution. The mixture was evaporated for several hours in a water bath at 80°C with vigorous stirring until a thick homogeneous gel was obtained. The gel precursors were vacuum freeze dried for 24 hr for the removal of residual water to produce the white solid product. The resulting solid product was successively calcined at 300°C for 3 hr and calcined at 900°C for another 12 hr in a tube furnace under a N_2 atmosphere with intermediate sufficient ball milling. The as-prepared $\text{NaTi}_2(\text{PO}_4)_3$ powder was coated with carbon through chemical vapor deposition. The obtained powder was calcined at 700°C for 4 hr under a N_2 /toluene atmosphere and then heated up to 900°C without toluene for 2 hr to yield the final product $\text{NaTi}_2(\text{PO}_4)_3@\text{C}$. The spinnable CNT arrays were first synthesized by a typical chemical vapor deposition method. Al_2O_3 (3 nm) and Fe (1.2 nm) were sequentially deposited onto a silicon wafer as the catalyst. The electron beam evaporation rates of Al_2O_3 and Fe were 2 and 0.5 Å s^{-1} , respectively. Ethylene (flow rate of 90 sccm) was used as the carbon precursor. A mixture of Ar (flow rate of 400 sccm) and H_2 (flow rate of 30 sccm) was used as the carrier gas. The growth of CNT arrays took place at 740°C for 10 min in a tube furnace to yield the spinnable CNT arrays. The aligned CNT sheet was continuously dry-drawn out of the CNT array with a knife.

Material Characterization

XRD data for all samples were collected by Bruker D8 X-Ray Systems with a Cu K α radiation source ($\lambda = 1.5406$ Å). The morphology of the samples was characterized by SEM (JEOL JSM-6390) and TEM (JEOL JEM-2010). TG analysis was carried on the TG209F1 instrument with an O_2 flow.

Preparation of Film Electrodes and Belt-Shaped SIBs

The film electrodes were produced by the mixture of active materials (NMO or NTPO@C), conductive agent (AB), and binder (PTFE) in a mass ratio of 80:10:10 in isopropanol. The obtained slurry was rolled into films. After being dried at 120°C for 12 hr in air, the electrode films (1 × 5 cm) were then pressed onto soft stainless steel mesh (1 × 6 cm) onto which nickel tabs had been welded for electron conduction. The mass loadings of NMO and NTPO@C were about 10 and 6 mg cm^{-2} , respectively. The flexible SIBs were fabricated with a capacity ratio of NMO cathode and NTPO@C anode of 1:1.1 according to the specific capacity of NMO (46 mAh g^{-1}) and NTPO@C (88 mAh g^{-1}) at a current density of 0.2 A g^{-1} . This capacity ratio was set because the end potential of Na storage in the $\text{NaTi}_2(\text{PO}_4)_3$ anode is close to the hydrogen evolution potential. A small amount of capacity excess in the anode was used just to prevent the undesired hydrogen evolution

reaction on the anode. The anode and cathode electrode films were then stacked up with an electrolyte-wetted separator between them. Finally, the flexible belt-shaped SIB was sealed through a vacuum sealing process. The electrolytes used were 1 M Na_2SO_4 solution, normal saline, and DMEM for different belt-shaped SIBs.

Preparation of Fiber Electrodes and Fiber-Shaped SIBs

Before the preparation of the fiber-shaped electrodes, the active materials (NMO and NTPO@C) were dispersed in ethanol to yield suspensions at concentrations of 1.7 and 1 mg/mL, respectively. The suspensions were treated under probe sonication to form homogeneous suspensions before use. Aligned CNT sheets were continuously pulled out from the spinnable CNT array. Four layers of aligned CNT sheets with a width of 2 cm were stacked along the drawing direction on a PTFE plate. The suspensions were dropped onto the CNT sheets on PTFE until the stacked CNT sheets were entirely immersed. A spinning machine then twisted the aligned CNT sheets into composite yarns to produce the fiber-shaped CNT/NMO and CNT/NTPO@C composite electrodes, respectively. Weight percentages of NMO and NTPO@C in the fiber electrodes were 92.5% and 83.1%, respectively. The diameter of the electrodes was about 110 μm (NMO) and 100 μm (NTPO@C). For the electrochemical tests, fiber electrodes were connected with copper wires through conductive silver adhesives. The joint was covered with glue to prevent a short circuit. The fiber electrodes were then immersed in 1 M Na_2SO_4 solution to afford the final fiber-shaped aqueous SIBs. Normal saline and DMEM were also used as aqueous electrolytes for building fiber-shaped SIBs by the same method. It should be noted that aqueous electrolytes for fiber-shaped SIBs must be pre-treated with a flow of N_2 for the removal of dissolved O_2 .

Electrochemical Measurements

The three-electrode systems used a Ag/AgCl electrode ($E = 0.1971$ V versus SHE) as the reference electrode. An activated carbon electrode was used as the counter electrode. Full cells were tested with a two-electrode system. The CV measurements of the samples were carried out on a CH Instruments electrochemical workstation (CHI 660D) at a scan rate of 1 mV s^{-1} . Galvanostatic charge-discharge and cycling stability tests were performed on a computer controlled by a Hukuto Denko battery charge-discharge system (HJ series). Electrochemical windows were between 0 and -0.9 V (versus Ag/AgCl) for the NTPO@C-containing electrode, between 0 and 0.7 V (versus Ag/AgCl) for the NMO-containing electrode, and 0 and 1.6 V for the full cell. All electrochemical tests (except CV) for the NTPO@C-containing electrodes and fiber-shaped SIBs were carried out with vigorously bubbling N_2 for the removal of dissolved O_2 in the electrolytes.

SUPPLEMENTAL INFORMATION

Supplemental Information includes Supplemental Experimental Procedures, 18 figures, and 2 tables and can be found with this article online at <http://dx.doi.org/10.1016/j.chempr.2017.05.004>.

AUTHOR CONTRIBUTIONS

Y.W. and H.P. conceived and designed the experiments. Z.G. prepared the electrode materials, corresponding film electrodes, and belt-shaped SIBs and carried out the electrochemical experiments. Y.Z. and J.C. prepared the fiber electrodes and fiber-shaped SIBs and performed the measurements. X.D. and L.C. assisted Z.G. in preparing the film electrodes and characterizing materials. Y.D. and C.W. assisted Y.Z. in preparing the DMEM solution. Y.X. gave some suggestions for the experimental design and data analysis for this work. Z.G., Y.Z., Y.W., and

H.P. co-wrote the paper. All authors discussed the results and commented on the manuscript.

ACKNOWLEDGMENTS

The authors acknowledge funding support from the Natural Science Foundation of China (21622303 and 21373060) and the State Key Basic Research Program of China (2016YFA0203302).

Received: March 13, 2017

Revised: April 12, 2017

Accepted: May 4, 2017

Published: August 10, 2017

REFERENCES AND NOTES

- Gao, W., Emaminejad, S., Nyein, H., Challa, S., Chen, K., Peck, A., Fahad, H.M., Ota, H., Shiraki, H., Kiriya, D., et al. (2016). Fully integrated wearable sensor arrays for multiplexed in situ perspiration analysis. *Nature* 529, 509.
- Yan, Y., Warren, S.C., Fuller, P., and Grzybowski, B.A. (2016). Chemo-electronic circuits based on metal nanoparticles. *Nat. Nanotechnol.* 11, 603–608.
- Feiner, R., Engel, L., Fleischer, S., Malki, M., Gal, I., Shapira, A., Shacham-Diamand, Y., and Dvir, T. (2016). Engineered hybrid cardiac patches with multifunctional electronics for online monitoring and regulation of tissue function. *Nat. Mater.* 15, 679–685.
- Kim, C.-C., Lee, H.-H., Oh, K.H., and Sun, J.-Y. (2016). Highly stretchable, transparent ionic touch panel. *Science* 353, 682–687.
- Zhang, Y., Zhao, Y., Ren, J., Weng, W., and Peng, H.S. (2016). Advances in wearable fiber-shaped lithium-ion batteries. *Adv. Mater.* 28, 4524–4531.
- Zhou, G.M., Li, F., and Cheng, H.M. (2014). Progress in flexible lithium batteries and future prospects. *Energy Environ. Sci.* 7, 1307–1338.
- Li, L., Wu, Z., Yuan, S., and Zhang, X.B. (2014). Advances and challenges for flexible energy storage and conversion devices and systems. *Energy Environ. Sci.* 7, 2101–2122.
- Gwon, H., Hong, J., Kim, H., Seo, D.-H., Jeon, S., and Kang, K. (2014). Recent progress on flexible lithium rechargeable batteries. *Energy Environ. Sci.* 7, 538–551.
- Armand, M., and Tarascon, J.-M. (2008). Building better batteries. *Nature* 451, 652–657.
- Simon, P., and Gogotsi, Y. (2008). Materials for electrochemical capacitors. *Nat. Mater.* 7, 845–854.
- Hu, Y.H., and Sun, X.L. (2014). Flexible rechargeable lithium ion batteries: advances and challenges in materials and process technologies. *J. Mater. Chem. A* 2, 10712–10738.
- Gaikwad, A.M., Khau, B.V., Davies, G., Hertzberg, B., Steingart, D.A., and Arias, A.C. (2015). A high areal capacity flexible lithium-ion battery with a strain-compliant design. *Adv. Energy Mater.* 5, 1401389.
- Zhang, Y., Bai, W.Y., Cheng, X.L., Ren, J., Weng, W., Chen, P.N., Fang, X., Zhang, Z.T., and Peng, H.S. (2014). Flexible and stretchable lithium-ion batteries and super-capacitors based on electrically conducting carbon nanotube fiber springs. *Angew. Chem. Int. Ed.* 53, 14564–14568.
- Ren, J., Zhang, Y., Bai, W.Y., Chen, X.L., Zhang, Z.T., Fang, X., Weng, W., Wang, Y.G., and Peng, H.S. (2014). Elastic and wearable wire-shaped lithium-ion battery with high electrochemical performance. *Angew. Chem. Int. Ed.* 53, 7864–7869.
- Chen, Z., To, J.W.F., Wang, C., Lu, Z.D., Liu, N., Chortos, A., Pan, L.J., Wei, F., Cui, Y., and Bao, Z.N. (2014). A three-dimensionally interconnected carbon nanotube-conducting polymer hydrogel network for high-performance flexible battery electrodes. *Adv. Energy Mater.* 4, 1400207.
- Kwon, Y.H., Woo, S.-W., Jung, H.-R., Yu, H.K., Kim, K., Oh, B.H., Ahn, S., Lee, S.-Y., Song, S.-W., Cho, J., et al. (2012). Cable-type flexible lithium ion battery based on hollow multi-helix electrodes. *Adv. Mater.* 24, 5192–5197.
- Li, N., Chen, Z.P., Ren, W.C., Li, F., and Cheng, H.-M. (2012). Flexible graphene-based lithium ion batteries with ultrafast charge and discharge rates. *Proc. Natl. Acad. Sci. USA* 109, 17360–17365.
- Hu, L.B., Wu, H., Mantia, F.L., Yang, Y., and Cui, Y. (2010). Thin, flexible secondary Li-ion paper batteries. *ACS Nano* 4, 5843–5848.
- Liu, S.H., Wang, Z.Y., Yu, C., Wu, H.B., Wang, G., Dong, Q., Qiu, J.S., Eychmüller, A., and Lou, X.W. (2013). A flexible TiO₂(B)-based battery electrode with superior power rate and ultralong cycle life. *Adv. Mater.* 25, 3462–3467.
- Dong, X.L., Chen, L., Su, X.L., Wang, Y.G., and Xia, Y.Y. (2016). Flexible aqueous lithium-ion battery with high safety and large volumetric energy density. *Angew. Chem. Int. Ed.* 55, 7474–7477.
- Zhou, G.M., Li, L., Wang, D.-W., Shan, X.-Y., Pei, S.F., Li, F., and Cheng, H.-M. (2015). A flexible sulfur-graphene-polypropylene separator integrated electrode for advanced Li-S batteries. *Adv. Mater.* 27, 641–647.
- Wu, F.X., Zhao, E., Gordon, D., Xiao, Y.R., Hu, C.C., and Yushin, G. (2016). Infiltrated porous polymer sheets as free-standing flexible lithium-sulfur battery electrodes. *Adv. Mater.* 28, 6365.
- Wang, H.Q., Zhang, W.C., Liu, H.K., and Guo, Z.P. (2016). A strategy for configuration of an integrated flexible sulfur cathode for high-performance lithium-sulfur batteries. *Angew. Chem. Int. Ed.* 55, 3992–3996.
- Liu, Q.-C., Xu, J.-J., Xu, D., and Zhang, X.-B. (2015). Flexible lithium-oxygen battery based on a recoverable cathode. *Nat. Commun.* 6, 7892.
- Zhang, Y., Wang, L., Guo, Z.Y., Xu, Y.F., Wang, Y.G., and Peng, H.S. (2016). High-performance lithium-air battery with a coaxial-fiber architecture. *Angew. Chem. Int. Ed.* 55, 4487–4491.
- Chen, T., Hao, R., Peng, H.S., and Dai, L.M. (2015). High-performance, stretchable, wire-shaped supercapacitors. *Angew. Chem. Int. Ed.* 54, 618–622.
- Yu, D.S., Goh, K., Wang, H., Wei, L., Jiang, W.C., Zhang, Q., Dai, L.M., and Chen, Y. (2014). Scalable synthesis of hierarchically structured carbon nanotube-graphene fibres for capacitive energy storage. *Nat. Nanotechnol.* 9, 555–562.
- Yang, Z.B., Deng, J., Chen, X.L., Ren, J., and Peng, H.S. (2013). A highly stretchable, fiber-shaped supercapacitor. *Angew. Chem. Int. Ed.* 52, 13453–13457.
- Dong, X.L., Guo, Z.Y., Song, Y.F., Hou, M.Y., Wang, J.Q., Wang, Y.G., and Xia, Y.Y. (2014). Flexible and wire-shaped micro-supercapacitor based on Ni(OH)₂-nanowire and ordered mesoporous carbon electrodes. *Adv. Funct. Mater.* 24, 3405–3412.
- Zhu, M.S., Huang, Y., Deng, Q.H., Zhou, J., Pei, Z.X., Xue, Q., Huang, Y., Wang, Z.F., Li, H.F., Huang, Q.H., et al. (2016). Highly flexible, freestanding supercapacitor electrode with enhanced performance obtained by hybridizing polypyrrole chains with mxene. *Adv. Energy Mater.* 6, 1600969.
- Hu, L.B., Chen, W., Xie, X., Liu, N., Yang, Y., Wu, H., Yao, Y., Pasta, M., Alshareef, H.N., and Cui, Y. (2011). Symmetrical MnO₂-carbon nanotube-textile nanostructures for wearable

- pseudocapacitors with high mass loading. *ACS Nano* 5, 8904–8913.
32. Gao, W., Singh, N., Song, L., Liu, Z., Reddy, A.L.M., Ci, L.J., Vajtai, R., Zhang, Q., Wei, B.Q., and Ajayan, P.M. (2011). Direct laser writing of micro-supercapacitors on hydrated graphite oxide films. *Nat. Nanotechnol.* 6, 496–500.
 33. Kim, S.-W., Seo, D.-H., Ma, X.H., Ceder, G., and Kang, K. (2012). Electrode materials for rechargeable sodium-ion batteries: potential alternatives to current lithium-ion batteries. *Adv. Energy Mater.* 2, 710–721.
 34. Guo, S.H., Yi, J., Sun, Y., and Zhou, H.S. (2016). Recent advances in titanium-based electrode materials for stationary sodium-ion batteries. *Energy Environ. Sci.* 9, 2978–3006.
 35. Wei, X., Li, W.H., Shi, J.-A., Gu, L., and Yu, Y. (2015). FeS@C on carbon cloth as flexible electrode for both lithium and sodium storage. *ACS Appl. Mater. Inter.* 7, 27804–27809.
 36. Liu, Y.C., Zhang, N., Jiao, L.F., and Chen, J. (2015). Tin nanodots encapsulated in porous nitrogen-doped carbon nanofibers as a free-standing anode for advanced sodium-ion batteries. *Adv. Mater.* 27, 6702–6707.
 37. Zhang, W., Liu, Y.T., Chen, C.J., Li, Z., Huang, Y.H., and Hu, X.L. (2015). Flexible and binder-free electrodes of Sb/rGO and Na₃V₂(PO₄)₃/rGO nanocomposites for sodium-ion batteries. *Small* 11, 3822–3829.
 38. Su, D.W., Dou, S.X., and Wang, G.X. (2014). WS₂@graphene nanocomposites as anode materials for Na-ion batteries with enhanced electrochemical performances. *Chem. Commun.* 50, 4192–4195.
 39. Wang, S.Q., Lu, X., Yu, L., Zhang, L., Wang, H.H., and Lou, X.W. (2016). Free-standing nitrogen-doped carbon nanofiber films: integrated electrodes for sodium-ion batteries with ultralong cycle life and superior rate capability. *Adv. Energy Mater.* 6, 1502217.
 40. Li, H.S., Peng, L.L., Zhu, Y., Zhang, X.G., and Yu, G.H. (2016). Achieving high-energy-high-power density in a flexible quasi-solid state sodium ion capacitor. *Nano Lett.* 16, 5938–5943.
 41. Li, Z., Young, D., Xiang, K., Carter, W.C., and Chiang, Y.M. (2013). Towards high power high energy aqueous sodium-ion batteries: the NaTi₂(PO₄)₃/Na_{0.44}MnO₂ system. *Adv. Energy Mater.* 3, 290–294.
 42. Hou, Z.G., Li, X.N., Liang, J.W., Zhu, Y.C., and Qian, Y.T. (2015). An aqueous rechargeable sodium ion battery based on a NaMnO₂-NaTi₂(PO₄)₃ hybrid system for stationary energy storage. *J. Mater. Chem. A* 3, 1400–1404.
 43. Whitacre, J.F., Tevar, A., and Sharma, S. (2010). Na₄Mn₉O₁₈ as a positive electrode material for an aqueous electrolyte sodium-ion energy storage device. *Electrochem. Commun.* 12, 463–466.
 44. Wang, X.F., Liu, B., Liu, R., Wang, Q.F., Hou, X.J., Chen, D., Wang, R.M., and Shen, G.Z. (2014). Fiber-based flexible all-solid-state asymmetric supercapacitors for integrated photodetecting system. *Angew. Chem. Int. Ed.* 53, 1849–1853.
 45. Zhang, M., Atkinson, K.R., and Baughman, R.H. (2004). Multifunctional carbon nanotube yarns by downsizing an ancient technology. *Science* 306, 1358–1361.
 46. Guo, W.H., Liu, C., Zhao, F.Y., Sun, X.M., Yang, Z.B., Chen, T., Chen, X.L., Qiu, L.B., Hu, X.H., and Peng, H.S. (2012). A novel electromechanical actuation mechanism of a carbon nanotube fiber. *Adv. Mater.* 24, 5379–5384.
 47. Zhao, Y., Zhang, Y., Sun, H., Dong, X.L., Cao, J.Y., Wang, L., Xu, Y.F., Ren, J., Hwang, Y., Son, I.H., et al. (2016). A self-healing aqueous lithium-ion battery. *Angew. Chem. Int. Ed.* 55, 14384–14388.
 48. Xu, Y.F., Zhang, Y., Guo, Z.Y., Ren, J., Wang, Y.G., and Peng, H.S. (2015). Flexible, stretchable, and rechargeable fiber-shaped zinc-air battery based on cross-stacked carbon nanotube sheets. *Angew. Chem. Int. Ed.* 54, 15390–15394.
 49. Zhang, C., Ni, D.L., Liu, Y.Y., Yao, H.L., Bu, W.B., and Shi, J.L. (2017). Magnesium silicide nanoparticles as a deoxygenation agent for cancer starvation therapy. *Nat. Nanotechnol.* 12, 378–386.
 50. Sauvage, F., Laffont, L., Tarascon, J.-M., and Baudrin, E. (2007). Study of the insertion/deinsertion mechanism of sodium into Na_{0.44}MnO₂. *Inorg. Chem.* 46, 3289–3294.
 51. Wang, Y.S., Liu, J., Lee, B.J., Qiao, R.M., Yang, Z.Z., Xu, S.Y., Yu, X.Q., Gu, L., Hu, Y.S., Yang, W.L., et al. (2015). Ti-substituted tunnel-type Na_{0.44}MnO₂ oxide as a negative electrode for aqueous sodium-ion batteries. *Nat. Commun.* 6, 6401.
 52. Chen, L., Liu, J.Y., Guo, Z.W., Wang, Y.G., Wang, C.X., and Xia, Y.Y. (2016). Electrochemical profile of LiTi₂(PO₄)₃ and NaTi₂(PO₄)₃ in lithium, sodium or mixed ion aqueous solutions. *J. Electrochem. Soc.* 163, A904–A910.
 53. Luo, J.-Y., Chen, L.-J., Zhao, Y.-J., He, P., and Xia, Y.-Y. (2009). The effect of oxygen vacancies on the structure and electrochemistry of LiTi₂(PO₄)₃ for lithium-ion batteries: a combined experimental and theoretical study. *J. Power Sources* 194, 1075–1080.